REGULAR ARTICLE

Efficient, Breathable and Biodegradable Filter Media for Face Masks

Xiaomin Zhang[1] · Yuanqiang Xu[1] · Yongchun Zeng[1]

Abstract

The global outbreak of COVID-19 results in the surge of disposable sanitary supplies, especially personal protective face masks. However, the charge dissipation of the electret meltblown nonwovens, which predominate in the commercial face mask filters, confines the durability and safety of commercial face masks. Furthermore, most of the face masks are made from nondegradable materials (such as PP) or part of their degradation products are toxic and contaminative to the environment. Herein, a type of face mask with biodegradable and highly effective PLA bi-layer complex fibrous membrane as filter core is reported. The prepared PLA complex membrane possesses a high-filtration efficiency of 99.1% for $PM_{0.3}$ while providing a favorable pressure drop of 93.2 Pa. With the PLA complex membrane as the filter core, our face mask exhibits comparable or even higher wearability to commercial face masks, which further manifests our designed PLA complex membrane a promising filter media for face masks.

Keywords Electrospinning · Air filtration · Face masks

1 Introduction

As a physical separation barrier on the exhaled droplets, face masks have become one of the essential personal protective equipment in people's daily life since the outbreak of the new coronavirus (COVID-2019) epidemic [1, 2]. A face mask usually consists of spunbonded nonwovens being the supporting layer (due to their robust mechanic strength) and electret meltblown nonwovens as the crucial filter core (taking advantage of small fiber dimeters, interconnective pore structure, high porosity and electrostatic adsorption) [3, 4]. Besides, particular matter (PM) air pollution has been progressively worse with the quick growth of urbanization and industrialization; thus, has adversely harmed nature and human health, leading to increased mortality and morbidity [5, 6]. Personal protective face masks can effectively protect people from inhaling hazardous PMs.

Electret meltblown nonwovens are the crucial filter core of face masks. By virtue of electrostatic adsorption effect, electret meltblown nonwovens can easily achieve high-filtration efficiency at low air resistance. Nevertheless, electret

meltblown nonwovens are susceptible to harsh circumstance, such as high humidity and temperature, where charge dissipation occurs, leading to a dramatic drop in filtration efficiency [2, 7]. On the other hand, the surge in the usage of disposable face masks, most of which made from nondegradative materials (such as PP and PE), and whose degradation products contains toxic substances, really burdens the self-purification of our earth [8–10].

Considering the unstable filtration efficiency of the electret meltblown nonwovens, many efforts have been taken from both academic and industry to explore fibrous filters without electret treatment. Nano-scaled fibers, which have variety of applications, can be manufactured through methods like electrospinning and blow spinning. Blow spinning is a new type of method developed from electrospinning and melt blown technology, which has variety of advantages like high-production efficiency and good safety [11, 12]. Although electrospinning was chosen for this study due to its well-established capability to produce high-quality, uniform nanofibers, which has been extensively studied and reported in many literatures. Electrospun fibers, with fiber diameter reaching to tens of nanometers, combined with diverse fiber morphology, have been an ever-increasing interest to the researchers as promising air filtration media [13–15]. By controlling the surface chemistry to enable strong PMs adhesion and also the microstructure of the air filters to increase

✉ Yongchun Zeng
yongchun@dhu.edu.cn

1 College of Textiles, Donghua University, Shanghai 201620, China

the capture possibilities, Cui and coworkers [16] achieved transparent, high-effective air filters of ~90% transparency with >95% removal of PM$_{2.5}$ under extreme hazardous air-quality conditions. Kang and coworkers [17] fabricated tree-like structured PLA nanofiber membranes through governing solvent type and amount of additive. The obtained PLA nanofiber membrane has a filtration efficiency of 99.89% with resistance of about 96.08 Pa. Using a capacity-like electronetting technology, which is by controlling the ejection, deformation, and phase separation of charged droplets from a Taylor cone, Ding and coworkers [18] created ultralight, thin, rubbery, self-assembled nanonetworks with high-efficiency and transparency as air filters. Huang and coworkers [19] produced eco-friendly curved-ribbon nanofiber membrane with multihierarchical structure based on green one-step electrospinning. The produced curved-ribbon nanofiber membrane exhibits high-filtration performance while maintain a low pressure drop.

As mentioned above, it is a worthy of studying strategy to explore promising air filters by means of regulating the fiber structure of fibrous filters. Herein, we fabricate electrospun PLA fibers with porous and wrinkled structure via governing solvent system of the polymer precursor solution. The effect of solvent ratio of dichloromethane (DCM) and ethyl alcohol (EtOH) on fiber morphology is studied to achieve optimal porous and wrinkle structured PLA fibers. Further, the filtration performances of the obtained PLA fibrous membranes with different thicknesses and distinct fiber structures are evaluated to obtain an optimal combination of bi-layer fibrous membrane as the filter core. The optimal PLA complex membrane is assembled as the filter core with two layers of spunbonded nonwovens to make a face mask. The tensile strength, air permeability and moisture permeability of the prepared face mask are tested to evaluate its wearable performances as a personal protective face mask. Moreover, the degradability of the PLA complex membrane is also demonstrated through enzymolysis experiment.

2 Experimental

2.1 Materials

Polylactic acid (PLA, 4032D) was purchased from the NatureWorks Company, USA. Dichloromethane (DCM) and anhydrous ethanol (EtOH) were from Sinopharm Group Chemical Reagent Co., Ltd., China. Proteinase K and PBS buffer solution were purchased from Fujian Lingjiang Biotechnology Co., Ltd., China. All chemicals were used as received without any purification.

Polypropylene (PP) spunbonded nonwovens and Polyethylene (PE) spunbonded nonwovens were obtained from Anhui Kangtai Nonwoven fabric Co., Ltd., China. N95 face masks were purchased from 3M China Co., Ltd. Surgical masks were supplied by Zhende medical Co., Ltd., China.

2.2 Sample Preparation

6 wt.% PLA electrospinning solutions with binary solvent system of DCM/EtOH (6:4, 7:3, 8:2, w/w) were prepared in two steps. PLA granules were dissolved into DCM and the mixtures were stirred for 3 h, and EtOH was added into afterwards and stirred until a transparent solution formed.

PLA solution prepared was extruded into syringe connected with a flat-tipped 22-gauge needle, and mounted on an infusion syringe pump with a fixed feed rate of 2 ml/h. The distance from the needle tip to the collector drum was kept at 15 cm. The applied voltage varies from 15 to 30 kV. The charged solution was then accelerated to the collector with a rotating speed of 60 r/min. The experiments were conducted at a 20 ± 5 ℃ temperature in a $50 \pm 5\%$ relative humidity.

The face masks were assembled by an industrial computer sewing machine (S-7200C-303A-G10, Brother). The electrospun PLA membranes were placed between PE and PP spunbonded nonwovens, which were then sewed up to get face masks.

2.3 Characterization

Samples of the as-spun PLA fibers were observed under Field Emission Scanning Electron Microscope (FE-SEM, SU8010, HITACHI) at an acceleration voltage of 5 kV after spluttered with platinum for 70 s. The average dimeter was calculated from 100 fibers measured by Image-Pro Plus software through SEM images. The thicknesses of the samples were measured by a thickness gauge from Aice Instrument Co., Ltd., China.

LZC-K filter tester from Suzhou Huada Filter Instrument and Equipment Co., Ltd., China was employed to evaluate the filtration performance of the samples. The NaCl aerosol particles with diameters of $0.26 - 10$ μm and a geometric standard deviation of < 1.86 were generated using a QRJ-1 stomizer from 2 wt% NaCl solutions. And, these PM particles were charge neutralized before fed into the filter holder for filter testing. Air flow with NaCl aerosol particles passed through the samples at a flow rate of 32 L min^{-1} (i.e., 5.3 cm s^{-1}) in an effective testing area of 100 cm^2. The concentration of NaCl aerogel particles can be adjusted by injecting air into the filter holder, while a particle counter can accurately identify particle size. Thus, the filtration efficiency of the samples was collected by comparing the number of PM in the upstream and downstream of the particle airflow. In addition, their pressure drop across the upstream and downstream sides of the samples can be measured using respective electronic

pressure transducers. The quality factor (QF) was used as the figure of merit to evaluate the filtration performance, which was calculated using the following formula [3, 20–22]:

$$QF = \frac{-\ln(1 - \eta)}{\Delta P} \tag{1}$$

With η representing the filtration efficiency and ΔP representing the pressure drop across the filter.

An electronic fabric strength tester (YG026MB, Wenzhou Fangyuan Instrument Co., Ltd., China) was employed to study the mechanical properties of the samples. Samples with dimension of 20 mm × 50 mm were mounted on the testing device with initial measurement distance of 30 mm and testing speed of 30 mm min^{-1}.

An automatic ventilation meter (YG461G, Ningbo Textile Instrument Factory, China) was used at ambient temperature to examine the air permeability of the samples. The tests were conducted under testing pressure of 200 Pa with testing area of 20 cm^2.

The water vapor transmission rates (WVTR) of the samples were tested by a computerized fabric moisture permeability meter (FX3180, TEXTEST, Switzerland) according to GB/T 12,704.1–2009.

The thermal stability of the sample was evaluated with the help of thermogravimetric analysis instrument (TGA 8000, PerkinElmer).

The water contact angle (WCA) was measured by a contact angle measuring instrument (OCA15EC, DataPhysics Instruments GmbH, Germany).

Proteinase K was used to investigate the enzymatic degradation of the sample. The sample was immersed in the 10 × PBS solution (pH = 9.0–9.5) with proteinase K concentration of 0.5 mg/ml at 60 ℃. The degradation process was recorded by weighing the sample every 1 h and taking photos every 3 h. The percentage of weight loss (WL) during degradation was calculated using the following formula [9]:

$$WL = \frac{M_b - M_a}{M_b} \tag{2}$$

where M_b and M_a are the weights of the sample before and after degradation, respectively.

3 Results and Discussion

3.1 The Morphology of Electrospun PLA fibers

To improve the filtration performance of the electrospun fibers, we set about endowing fibers with special morphologies by introducing nonsolvent into solvent system, which is later confirmed to have a great impact on the obtained PLA fiber morphology. To elaborate, we governed the solvent mass ratio to observe the obtained PLA fibers. PLA was dissolved in three binary solvents with diverse mass ratios (DCM: EtOH) of 6:4, 7:3 and 8:2, separately. The solvent mass ratio of DCM: EtOH is abbreviated as D:E to be conciseness in the following instruction. These three PLA polymer solutions were then electrospun under the same applied voltage of 25 kV. The SEM images of the prepared PLA fibers are shown in Fig. 1. When D:E comes to 6:4, the fiber surface exhibits large amounts of pores and wrinkles, which we name as 'PLA porous-wrinkled fiber'. When raise the D:E to 7:3, the fiber surface becomes comparatively even with a spot of wrinkles on it, and pores disappear. Further increasing the D:E to 8:2, only wrinkles exist in fiber surface, similar to that of D:E of 7:3.

PLA is insoluble in EtOH, in other words, EtOH is a nonsolvent to PLA in binary solvent mentioned above. In the homogenous ternary solution system (i.e., polymer, solvent, and nonsolvent), DCM and EtOH evaporate at different speed due to diverse boiling points of DCM (39.8 ℃) and EtOH (78.5 ℃) at standard atmosphere pressure. During electrospinning, DCM evaporates faster than EtOH. The incoordinated evaporation between DCM and EtOH give rises to the uneven collapses of the solid skin under the
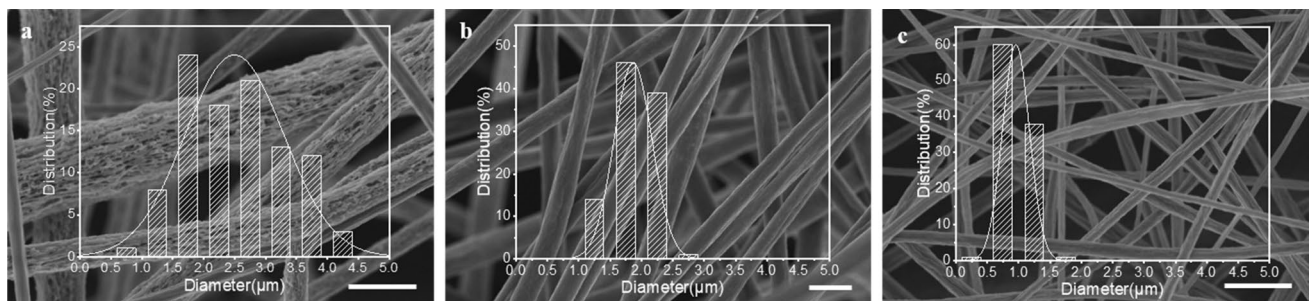
Fig. 1 SEM images of PLA fibrous membranes fabricated with D:E of **a** 6:4; **b** 7:3; **c** 8:2; the inserted images are the corresponding fiber diameter distributions. Scale bars are 5 μm

atmospheric pressure, which develop into wrinkles on the fiber surface when evaporation is completed. When boosting the proportion of nonsolvent (EtOH) to a certain value, non-solvent remains in the system during solidification, where phase separation occurs, leading to nonsolvent-rich phases and polymer-rich phases. Pores form along with the evaporation of nonsolvent, leaving the porous-wrinkled structures on the fiber surface [23].

Notably, the fiber diameter varies with the increase of the D:E. Figure 1d displays the diameter distribution of the PLA fibers prepared from D:E of 6:4, 7:3, and 8:2, whose average diameters are 2.50 µm, 1.87 µm, and 0.96 µm, respectively. With the decrease of proportion of EtOH, the obtained fibers become thinner and have narrower distribution. It takes more time to complete evaporation and solidification during electrospinning due to the increase of DCM in polymer solution, contributing to extended drawing of jet. Besides, agglomeration appears easily at the spinneret when D:E is 8:2, which attributes to the fast phase separation between DCM and EtOH resulting from the small proportion of EtOH.

3.2 Filtration Performance of the PLA Fibrous Membrane

The mechanism underlying the particle capture ability of our membrane, which comprises porous and wrinkled fibers, is primarily based on mechanical filtration. This process mainly involves the physical phenomena of inertial impaction, interception, and diffusion. Moreover, the fibrous morphologies of the membrane, characterized by porous and wrinkled surfaces, amplify the inter-fiber friction with particulate matter (PM) owing to the presence of finer-scale roughness associated with the pores and wrinkles. In addition, the pore and wrinkle structures of the fibers feature deep grooves, which provide supplementary pathways for PM capture.

The particle capture mechanism of the porous and wrinkled fibers is schematic shown in Fig. 2.
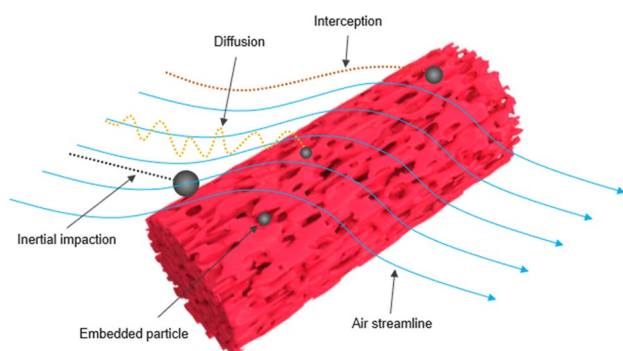
Fig. 2 A schematic explaining the filtration mechanism

3.2.1 The Filtration Performance of Monolayer PLA Fibrous Membrane

The filtration performances of PLA fibrous membranes prepared with different solvent systems for NaCl PMs are displayed in Table 1. Although fibrous membranes prepared from D:E of 8:2 (D:E-8:2) exhibits the best quality factor, the occurrence of agglomeration around the spinneret during spinning process hinders from collecting sufficient amounts of fibers, which brings about its low filtration efficiency. The fibrous membrane prepared from D:E of 7:3 (D:E-7:3) exerts the highest filtration efficiency among three of them. The filtration efficiency of D:E-7:3 outperforms that of fibrous membrane prepared by D:E of 6:4 (D:E-6:4), which is attributed to the smaller diameter of D:E-7:3 (average diameter of 1.87 µm), while the average fiber diameter of D:E-6:4 is 2.5 µm. The thicknesses of the testing fibrous membranes are 16 µm (D:E-6:4) and 15 µm (D:E-7:3), respectively, prepared with the same spinning time of 20 min. Under the circumstance of similar thickness, the pore size of the membrane diminishes with the decrease of fiber diameter, contributing to higher filtration efficiency [24]. On the other hand, smaller fibers caused minor pore sizes lead to an increment in pressure drop, which gives rise to the low quality factor of D:E-7:3 despite its highest filtration efficiency.

The thickness of PLA fibrous membrane is directly correlated to the spinning time. The filtration performances of PLA fibrous membranes prepared with unequal spinning time on NaCl $PM_{0.3}$ are tested, which are generalized in Tables 2 and 3, corresponding to D:E-6:4 and D:E-7:3,

Table 1 Filtration performance on NaCl $PM_{0.3}$ of PLA fibrous membranes prepared from diverse solvent mass ratios

Solvent mass ratio of DCM/EtOH	Filtration efficiency (%)	Pressure drop (Pa)	Quality factor (Pa^{-1})
6:4	70.30	29.0	0.0419
7:3	81.31	51.0	0.0329
8:2	51.48	15.8	0.0460

Table 2 Filtration performance on NaCl $PM_{0.3}$ of D:E-6:4 prepared with different spinning times

Spinning time (min)	Basis weight (g·m^{-2})	Filtration efficiency (%)	Pressure drop (Pa)	Quality factor (Pa^{-1})
20	1.36	70.30	29.0	0.0419
30	2.06	78.74	39.7	0.0390
40	2.61	89.86	49.2	0.0465
50	3.49	93.74	64.0	0.0433
60	4.12	96.64	67.7	0.0501
70	4.79	98.89	101.7	0.0427

Table 3 Filtration performance on NaCl $PM_{0.3}$ of D:E-7:3 prepared with different spinning times

Spinning time (min)	Basis weight ($g \cdot m^{-2}$)	Filtration efficiency (%)	Pressure drop (Pa)	Quality factor (Pa^{-1})
10	0.87	67.36	36.3	0.0308
20	1.60	81.31	51.0	0.0329
30	2.18	85.73	52.5	0.0371
40	2.92	97.71	97.0	0.0389
50	3.51	98.02	103.0	0.0395
60	4.38	98.28	117.8	0.0345

Table 4 Filtration performance (NaCl $PM_{0.3}$) of PLA bi-layer complex membranes consisting of D:E-6:4 and D:E-7:3

Complex membrane	Filtration efficiency (%)	Pressure drop (Pa)	Quality factor (Pa^{-1})
D:E-6:4–60/ D:E-7:3–10	99.71	109.7	0.0532
D:E-6:4–60/ D:E-7:3–20	99.68	122.8	0.0468
D:E-6:4–60/ D:E-7:3–30	99.72	128.5	0.0456
D:E-6:4–60/ D:E-7:3–40	99.91	136.2	0.0521
D:E-6:4–60/ D:E-7:3–50	99.97	161.5	0.0508
D:E-6:4–20/ D:E-7:3–50	99.71	118.5	0.0494
D:E-6:4–30/ D:E-7:3–50	99.82	135.7	0.0565
D:E-6:4–40/ D:E-7:3–50	99.84	150.2	0.0429
D:E-6:4–50/ D:E-7:3–50	99.93	165.3	0.0440
D:E-6:4–40/ D:E-7:3–10	99.10	93.2	0.0505
D:E-6:4–40/ D:E-7:3–20	99.26	104.7	0.0469
D:E-6:4–40/ D:E-7:3–30	99.28	107.5	0.0459
D:E-6:4–40/ D:E-7:3–40	99.68	120.5	0.0478

respectively, where D:E-8:2 isn't involved due to its easy agglomeration during spinning process. For simplicity, D:E-6:4-*t* is used to refer to fibrous membrane prepared with spinning time of *t* min, so is D:E-7:3-*t*.

With the increase of spinning time, both filtration efficiency and pressure drop increase. There is a sharp increment of pressure drop from D:E-6:4–60 to D:E-6:4–70, resultantly the quality factor declines despite its steady growth from D:E-6:4–20 to D:E-6:4–60. In case of D:E-7:3, the quality factor first grows gradually from D:E-7:3–10 to D:E-7:3–50, then drops off from D:E-7:3–50 to D:E-7:3–60, which is owing to the little-to-no increment in the filtration efficiency accompanied by the steady growth in pressure drop.

3.2.2 The Filtration Performance of Bi-Layer Complex PLA Fibrous Membrane

Both the filtration efficiency of D:E-6:3 and D:E-7:3 can hardly be improved by further increasing the membrane thickness without the sacrifice of pressure drop. According to the comprehensive filtration performance (i.e., quality factor), D:E-6:4–60 (D:E-7:3–50) is picked out to combine with D:E-7:3 (D:E-6:4) with diverse thicknesses to form bi-layer complex membranes, whose filtration performances are explored then (Table 4).

A prominent improvement on filtration efficiency (up to 99.97%) for NaCl $PM_{0.3}$ is exhibited in the bi-layer complex membranes, as compared to monolayer PLA membranes (up to 98.89%). Meanwhile, there is a huge growth in pressure drop, up to 161.5 Pa^{-1}, which is detrimental to being a filter core in facemask. To reduce the pressure drop to a satisfying degree, complex membranes consisting of D:E-6:4–40 and D:E-7:3 are inspected for the filtration performance. The PLA bi-layer complex membrane of D:E-6:4–40/D:E-7:3–10 presents a high-filtration efficiency of 99.10% for $PM_{0.3}$, 99.26% for $PM_{0.3–0.5}$, 100% for $PM_{0.5–1}$, (Table S1 in Supplementary Material), and favorable pressure drop of 93.2 Pa^{-1}, so to speak, possesses an excellent comprehensive filtration performance (QF = 0.0505).

We further tested the filtration performance of the PLA bi-layer complex membrane ("D:E-6:4–40/D:E-7:3–10" is omitted here for conciseness, and the following descriptions are managed likewise) under diverse air flow rates, the results are shown in Fig. 3a. No significant decline (only slight drop off from 99.89 to 99.10%) in filtration performance is observed when raising the air flow rate from 8 to 32 L min^{-1}. A relatively large drop of filtration efficiency happens when increasing the air flow rate to 45 L min^{-1}, which is considered faster than the air flow rate of breathing. As shown in Fig. 3c, after 30 cycles of filtration tests, the PLA bi-layer complex membrane maintains a consistent filtration efficiency and exhibits a barely visible increase in pressure drop, demonstrating excellent cycling utilization.

Soft oil particles (di(2-ethylhexyl) sebacate, DEHS PM) are employed to study the filtration performance of the aforementioned PLA bi-layer complex membrane for oil particles. The results are demonstrated in Fig. 3b, where the PLA bi-layer complex membrane exhibits high-filtration efficiency of 98.76% for DEHS $PM_{0.3}$, 98.91% for DEHS $PM_{0.3–0.5}$ and 100% for DEHS $PM_{0.5–1}$, while keeping the pressure drop at a low value of 98.83 Pa^{-1}. In the removal process of soft oil particles (DEHS), the oil particles would move along the fiber and coalesce into large spherical particles or liquid films at the fiber intersections as the loading continuing, the resulting long-time agglomeration of DEHS PMs might penetrate across the membranes and break into small droplets due to the high-speed airflow. In addition, the polarity effect of DEHS can reduce the adhesion between PMs and fibers [18]. These two points may account for the slightly inferior filtration efficiency of the PLA bi-layer complex membrane for DEHS PMs than for NaCl PMs.
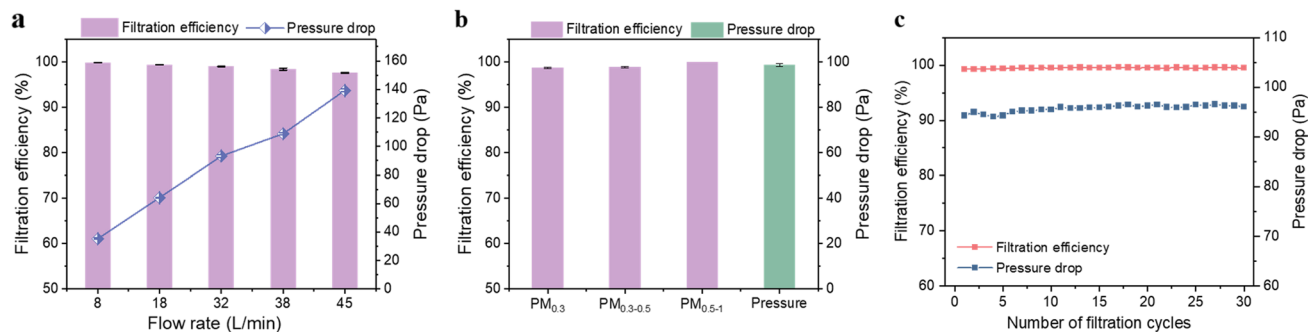
Fig. 3 Filtration performance of PLA bi-layer complex membrane (D:E-6:4–40/D:E-7:3–10) **a** on NaCl PM$_{0.3}$, tested under diverse air flow rates; **b** on DEHS PMs; **c** cycling filtration performance of the PLA bi-layer complex membrane

3.3 Wearability of the PLA Bi-layer Complex Membrane for Face Masks

The PLA complex membrane is used as the filter core to prepare a face mask. Apart from the filter core, PP and hydrophilic PE spunbonded nonwovens are employed as the supporting parts, where PE as the inner layer close to the face and PP as the outer layer close to the environment. The assembled face mask is displayed in Fig. 4a. The individual filtration performances of these two supporting layers are listed in Table S1 in the Supplementary Materials. For comparison, two commercial face masks, N95 face mask and surgical mask, are employed to assess the wearability of our face mask prepared in this work. Figure 4b shows the tensile

strength of the aforementioned three face masks, where we can see our face mask can endure tensile force comparable to N95 face mask, and higher than the surgical masks. Air permeability, the velocity of air traversing a sample under a certain pressure, is concerned with the pressure drop of a fibrous membrane filter. Our face mask has an air permeability comparable to the N95 face mask, as illustrated in Fig. 4c, given that our face mask has a high-filtration efficiency of 99.10%. The PLA bi-layer complex membrane starts to decompose at 297℃ (see Figure S1 in supplementary materials), which ensures its durability as a face mask in high-temperature environments. Breathing produced water vapor can bring discomfort while wearing face mask, where the WVTR represents the transmission rate of the moisture

Fig. 4 **a** Photo of the assembled face mask with the PLA bi-layer complex membrane as the filter core; **b** the comparison of tensile strength between commercial face masks and the face mask in this work; **c** the air permeability of the above face masks; **d** the WVTR test results of the above face masks
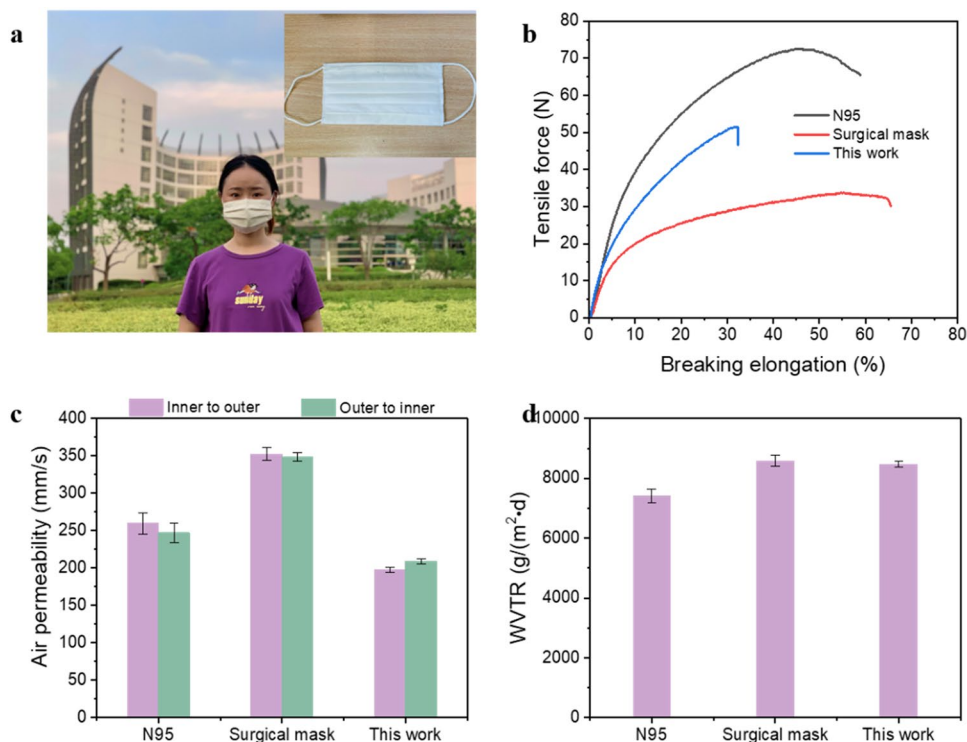
traversing the face mask to evaluate the wearability on one hand. The higher the WVTR, the faster the moisture is transferred out of the face mask, which can effectively mitigate the discomfort while wearing face mask. Notably our face mask exhibits a high WVTR, comparable to surgical face mask, while maintaining an excellent filtration efficiency. It is known that fiber membranes with poor water resistance can result in the deficiency of filtration performance under high humidity [25]. The PLA bi-layer complex membrane has a water contact angle (WCA) of 135° (see Figure S2 in supplementary materials), which ensures its filtration performance in humid environments. On the other hand, the great hydrophobicity enables the face mask to effectively prevent droplet penetration, which is crucial in reducing the risk of virus transmission as respiratory diseases are commonly spread through droplet transmission.

3.4 Biodegradability of the PLA Bi-layer Complex Membrane for Face Masks

The degradability of PLA complex membrane is investigated. Due to the long degradation lifetime of PLA, enzymolysis experiment is employed at a high temperature of 60℃ to accelerate the PLA complex membrane degradation. As shown in Fig. 5a, as time goes on, the PLA complex

membrane splits into fragments that diminish gradually until almost completely degraded. The PLA complex membrane is completely decomposed by proteinase K after 9 h (Fig. 5b). Figure 5c shows that the PLA complex membrane is partially degraded after 30 days outdoor soil burial. These outcomes confirm our membrane's biodegradability in a probable real-world setting. It is worth noting that the degradation products of PLA, such as CO_2 and H_2O, are all eco-friendly substances, which are harmless to the environment. Furthermore, the produced CO_2 and H_2O can be utilized by plants, which helps replenish the carbon cycle. The use of PLA as feedstock and the degradation of their products are expected to alleviate the environment pollution caused by other disposable hygiene products.

4 Conclusions

In summary, we have reported a biodegradable and highly effective PLA bi-layer complex fibrous membrane as filter core for face mask. Electrospun PLA fibrous membrane with porous-winkled structure is obtained via controlling the solvent system. Another electrospun PLA fibrous membrane without porous-wrinkled structure but having smaller fiber diameter and wrinkled surfaces is prepared as well.
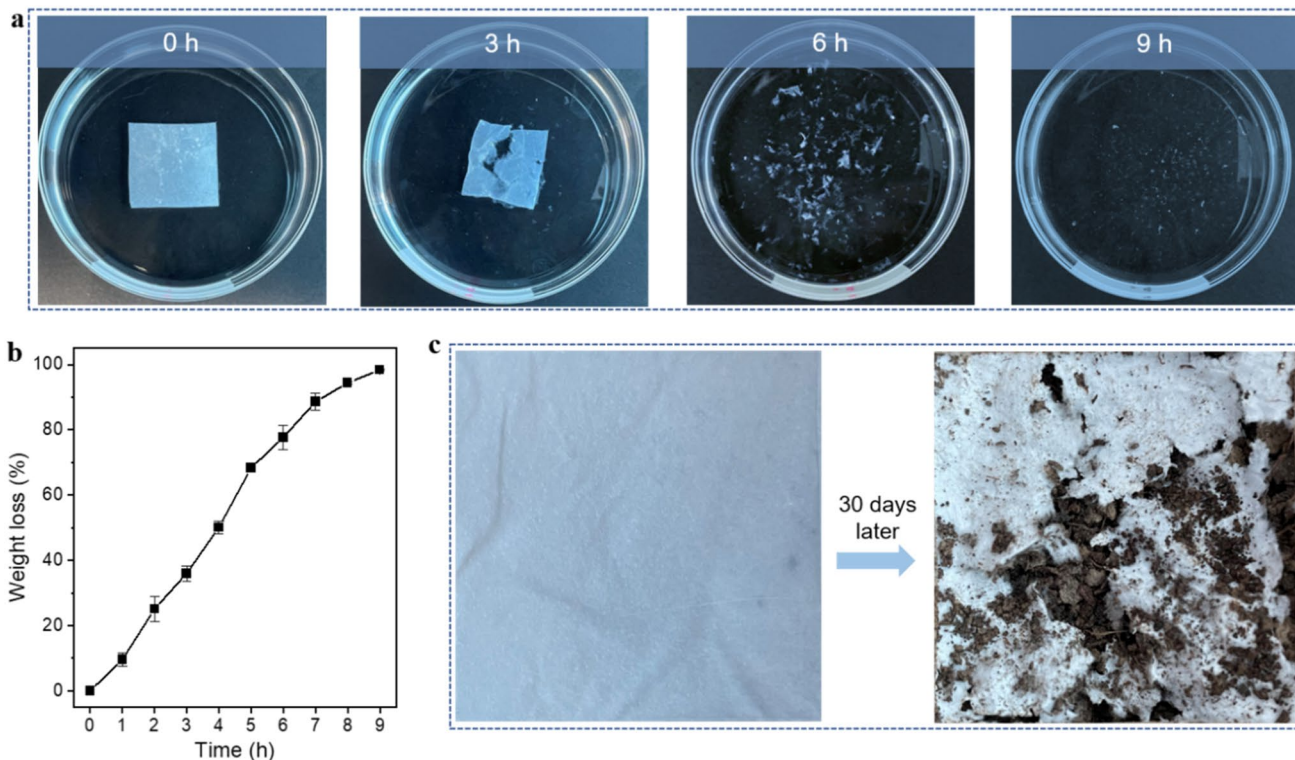
Fig. 5 a Time-dependent enzymatic degradation images of the PLA complex membrane and **b** the corresponding weight loss as a function of time; **c** images demonstrating the soil burial degradation of the PLA complex membrane

These two distinct PLA fibrous membranes are combined to achieve filtration performance outperform every single one. The resultant PLA bi-layer complex membrane exhibits a high-filtration efficiency for NaCl PMs, which is 99.10%, 99.26%, and 100% for $PM_{0.3}$, $PM_{0.3-0.5}$ and $PM_{0.5-1}$, respectively, and favorable pressure drop of 93.2 Pa^{-1}. In case of DEHS PMs, the filtration efficiency is 98.76%, 98.91% and 100%for $PM_{0.3}$, $PM_{0.3-0.5}$ and $PM_{0.5-1}$, respectively, with a low pressure drop of 98.83 Pa^{-1}. The assembled face mask exhibits comparable or even higher wearability (including tensile strength, air permeability and water vapor transmission) to two kinds of commercial face masks. The PLA complex membrane is demonstrated to be degradable through enzymolysis experiment, which indicating it a promising filter media for personal protective face masks, which is expected to alleviate environmental burdens to a certain extent.

Declarations

Conflict of Interest The authors declare no conflict of interest.

References

1. L. Liao, W. Xiao, M. Zhao, X. Yu, H. Wang, Q. Wang, S. Chu, Y. Cui, Can N95 respirators be reused after disinfection? How many times? ACS Nano **14**, 6348–6356 (2020). https://doi.org/10.1021/acsnano.0c03597

2. R.K. Campos, J. Jin, G.H. Rafael, M. Zhao, L. Liao, G. Simmons, S. Chu, S.C. Weaver, W. Chiu, Y. Cui, Decontamination of SARS-CoV-2 and Other RNA viruses from N95 level meltblown polypropylene fabric using heat under different humidities. ACS Nano (2020). https://doi.org/10.1021/acsnano.0c06565

3. J. Xu, X. Xiao, W. Zhang, R. Xu, S.C. Kim, Y. Cui, T.T. Howard, E. Wu, Y. Cui, Air-filtering masks for respiratory protection from PM2.5 and pandemic pathogens. One Earth. **3**, 574–589 (2020). https://doi.org/10.1016/j.oneear.2020.10.014

4. A. Ghosal, S. Sinha-Ray, A.L. Yarin, B. Pourdeyhimi, Numerical prediction of the effect of uptake velocity on three-dimensional structure, porosity and permeability of meltblown nonwoven laydown. Polymer **85**, 19–27 (2016). https://doi.org/10.1016/j.polymer.2016.01.013

5. Liu H. Structural design and fabrication of untrafine two-dimensional nanofaiber/nets for high-performance air filtration. PhD dissertation. Donghua University; 2020. doi:https://doi.org/10.27012/d.cnki.gdhuu.2020.000558

6. C.A. Pope, D.W. Dockery, Health effects of fine particulate air pollution: Lines that connect. J. Air Waste Manag. Assoc. **56**, 709–742 (2006). https://doi.org/10.1080/10473289.2006.10464545

7. T.A. Yovcheva, G.A. Mekishev, A.T. Marinov, A percolation theory analysis of surface potential decay related to corona charged polypropylene (PP) electrets. J. Phys. Condens. Matter. **16**, 455–464 (2004). https://doi.org/10.1088/0953-8984/16/3/021

8. E. Castro-Aguirre, F. Iñiguez-Franco, H. Samsudin, X. Fang, R. Auras, Poly(lactic acid)—mass production, processing, industrial applications, and end of life. Adv. Drug Deliv. Rev. **107**, 333–366 (2016). https://doi.org/10.1016/j.addr.2016.03.010

9. L. Wang, Y. Gao, J. Xiong, W. Shao, C. Cui, N. Sun, Y. Zhang, S. Chang, P. Han, F. Liu, J. He, Biodegradable and high-performance multiscale structured nanofiber membrane as mask filter media via poly(lactic acid) electrospinning. J. Colloid Interface Sci. **606**, 961–970 (2022). https://doi.org/10.1016/j.jcis.2021.08.079

10. E.G. Xu, Z.J. Ren, Preventing masks from becoming the next plastic problem. Front. Environ. Sci. Eng. **15**, 125 (2021). https://doi.org/10.1007/s11783-021-1413-7

11. C. Zhang, M. Chen, H. Li, W. Yang, J. Tan, The critical roles of the gas flow in fabricating polymer nanofibers: a mini-review. Adv. Fiber Mater. **4**, 162–170 (2022). https://doi.org/10.1007/s42765-021-00114-7

12. T. Lu, H. Liang, W. Cao, Y. Deng, Q. Qu, W. Ma, R. Xiong, C. Huang, Blow-spun nanofibrous composite Self-cleaning membrane for enhanced purification of oily wastewater. J. Colloid Interface Sci. **608**, 2860–2869 (2022). https://doi.org/10.1016/j.jcis.2021.11.017

13. T. Lu, J. Cui, Q. Qu, Y. Wang, J. Zhang, R. Xiong, W. Ma, C. Huang, Multistructured electrospun nanofibers for air filtration: a review. ACS Appl. Mater. Interfaces. **13**, 23293–23313 (2021). https://doi.org/10.1021/acsami.1c06520

14. A. Greiner, J.H. Wendorff, Electrospinning: A fascinating method for the preparation of ultrathin fibers. Angew. Chem. Int. Ed. **46**, 5670–5703 (2007). https://doi.org/10.1002/anie.200604646

15. H. Liu, C. Cao, J. Huang, Z. Chen, G. Chen, Y. Lai, Progress on particulate matter filtration technology: basic concepts, advanced materials, and performances. Nanoscale **12**, 437–453 (2020). https://doi.org/10.1039/c9nr08851b

16. C. Liu, P.-C. Hsu, H.-W. Lee, M. Ye, G. Zheng, N. Liu, W. Li, Y. Cui, Transparent air filter for high-efficiency PM25 capture. Nat. Commun. **6**, 6205 (2015). https://doi.org/10.1038/ncomms7205

17. B. Chen, L. Gao, S. Armadb, N. Deng, W. Kang, Fabrication of polylactic acid tree-like nanofiber membrane and its application in filtration. Journal of Textile Research (2018). https://doi.org/10.13475/j.fzxb.20180801206

18. S. Zhang, H. Liu, N. Tang, N. Ali, J. Yu, B. Ding, Highly efficient, transparent, and multifunctional air filters using self-assembled 2D Nanoarchitectured fibrous networks. ACS Nano **13**, 13501–13512 (2019). https://doi.org/10.1021/acsnano.9b07293

19. Y. Deng, T. Lu, X. Zhang, Z. Zeng, R. Tao, Q. Qu, Y. Zhang, M. Zhu, R. Xiong, C. Huang, Multi-hierarchical nanofiber membrane with typical curved-ribbon structure fabricated by green electrospinning for efficient, breathable and sustainable air filtration. J. Membr. Sci. **660**, 120857 (2022). https://doi.org/10.1016/j.memsci.2022.120857

20. Q. Wang, Y. Wei, W. Li, X. Luo, X. Zhang, J. Di, G. Wang, J. Yu, Polarity-dominated stable N97 respirators for airborne virus capture based on Nanofibrous membranes. Angew. Chem. Int. Ed Engl. **60**, 23756–23762 (2021). https://doi.org/10.1002/anie.202108951

21. H. Liu, J. Yu, S. Zhang, B. Ding, Air-conditioned masks using Nanofibrous networks for daytime radiative cooling. Nano Lett. **22**, 9485–9492 (2022). https://doi.org/10.1021/acs.nanolett.2c03585

22. Z. Peng, J. Shi, X. Xiao, Y. Hong, X. Li, W. Zhang, Y. Cheng, Z. Wang, W.J. Li, J. Chen, M.K.H. Leung, Z. Yang, Self-charging

electrostatic face masks leveraging triboelectrification for prolonged air filtration. Nat. Commun. **13**, 7835 (2022). https://doi.org/10.1038/s41467-022-35521-w

23. G.R. Guillen, Y. Pan, M. Li, E.M.V. Hoek, Preparation and characterization of membranes formed by nonsolvent induced phase separation: a review. Ind. Eng. Chem. Res. **50**, 3798–3817 (2011). https://doi.org/10.1021/ie101928r

24. Y. Xu, X. Zhang, X. Hao, D. Teng, T. Zhao, Y. Zeng, Micro/nanofibrous nonwovens with high filtration performance and radiative heat dissipation property for personal protective face mask. Chem. Eng. J. **423**, 130175 (2021). https://doi.org/10.1016/j.cej.2021.130175

25. Y. Deng, M. Zhu, T. Lu, Q. Fan, W. Ma, X. Zhang, L. Chen, H. Min, R. Xiong, C. Huang, Hierarchical fiber with granular-convex structure for highly efficient PM2.5 capture. Sep. Purif. Technol. **304**, 122235 (2023). https://doi.org/10.1016/j.seppur.2022.122235